Space Weather

RESEARCH ARTICLE
10.1029/2018SW001860

Special Section:
Space Weather Events of 4-10 September 2017

Shock Connectivity and the Late Cycle 24 Solar Energetic Particle Events in July and September 2017

J. G. Luhmann[1], M. L. Mays[2], Yan Li[1], C. O. Lee[1], H. Bain[3], D. Odstrcil[4], R. A. Mewaldt[5], C. M. S. Cohen[5], D. Larson[1], and Gordon Petrie[6]

[1]Space Sciences Laboratory, University of California, Berkeley, CA, USA, [2]CCMC, NASA Goddard Space Flight Center, Greenbelt, MD, USA, [3]NOAA Space Weather Prediction Center, Boulder, CO, USA, [4]Department of Physics and Astronomy, George Mason University, Fairfax, VA, USA, [5]Division of Physics, Mathematics and Astronomy, California Institute of Technology, Pasadena, CA, USA, [6]NSO, Boulder, CO, USA

Key Points:
- Observer shock connectivity explains the SEP observations during the July and September 2017 events
- The July and September 2017 solar and SEP events had similar characteristics due to similar source region and eruptions
- The July and September 2017 events seemed to arise in conjunction with the appearance of a pseudostreamer, a possible alternate ICME source

Correspondence to:
J. G. Luhmann,
jgluhman@ssl.berkeley.edu

Citation:
Luhmann, J. G., Mays, M. L., Li, Y., Lee, C. O., Bain, H., Odstrcil, D., et al. (2018). Shock connectivity and the late cycle 24 solar energetic particle events in July and September 2017. *Space Weather*, *16*, 557–568. https://doi.org/10.1029/2018SW001860

Received 6 MAR 2018
Accepted 28 APR 2018
Accepted article online 6 MAY 2018
Published online 25 MAY 2018

Abstract As solar activity steadily declined toward the cycle 24 minimum in the early months of 2017, the expectation for major solar energetic particle (SEP) events diminished with the sunspot number. It was thus surprising (though not unprecedented) when a new, potentially significant active region rotated around the East limb in early July that by midmonth was producing a series of coronal eruptions, reaching a crescendo around 23 July. This series, apparently associated with the birth of a growing pseudostreamer, produced the largest SEP event(s) seen since the solar maximum years. Activity abated with the decay of the active region, but a second episode of magnetic flux emergence in the same area in early September initiated a new round of eruptions. The western longitude of the erupting region, together with its similar coronal setting in both cases, resulted in a set of nearly homologous multipoint SEP event periods at Earth, Solar TErrestrial RElations Observatory-A and Mars (Mars Atmosphere and Volatile EvolutioN) for July and September 2017. We use a combination of WSA-ENLIL-cone heliospheric simulation results, together with SEPMOD SEP event modeling, to illustrate how the event similarities at the three observer sites can be understood from their relative positions and their connectivities to the generated interplanetary shocks.

1. Introduction

The decline of the already weak solar cycle 24 brought with it the expectation of diminishing solar energetic particle (SEP) activity with sunspot number. Indeed, after the STEREO (Solar TErrestrial RElations Observatory) mission was launched near the end of 2006 with its complement of imagers and in situ particles and fields instrumentation (Kaiser et al., 2008), the outlook for observing major SEP events during the 2-year prime mission was not good, given its timing in the late declining phase of cycle 23. The mission team was thus elated to see a major solar eruptive episode in December 2006 that produced an exceptionally intense SEP event for a period when active regions that harbor such outbursts are typically absent or largely decayed (von Rosenvinge et al., 2009). By the time the decline of cycle 24 was upon us this brief but intense late cycle 23 activity was largely forgotten with the occurrence of newer major events (Richardson et al., 2014), but in a coincidence that probably warrants space-weather interest, a similarly notable late cycle 24 active period accompanied by intense SEPs has now occurred again in July–September 2017. In this paper we consider the circumstances of these latter events and then use available modeling capabilities to illustrate how the occurrence of multiple coronal eruptions from the region of a persistent pseudostreamer probably led to the generation of multiple interplanetary shocks. Those in turn produced the significant SEP events detected at three widespread observer outposts at Earth (ACE [Advanced Composition Explorer] and GOES [Geostationary Operational Environmental Satellite Program]), STEREO-A, and Mars (Mars Atmosphere and Volatile EvolutioN [MAVEN]; Figure 1). In addition to contributing to studies of multiple eruptions in pseudostreamers as sources of large, multiple ICMEs (interplanetary coronal mass ejections) and their related SEP events, this study provides another example where observer shock magnetic connectivity is invoked to understand distributed, widespread multipoint SEP events.

The tools used here to develop the picture of the shocks and related SEPs for the late 2017 events consist of the combination of WSA-ENLIL-cone data-driven magnetohydrodynamic (MHD) simulation results available at the CCMC (Community Coordinated Modeling Center) and the SEPMOD solar energetic proton event model whose status was recently reviewed in Space Weather (Luhmann et al., 2017). Here we briefly describe the essentials of using the WSA-ENLIL-cone (alternately referred to here as ENLIL) and SEPMOD-combined

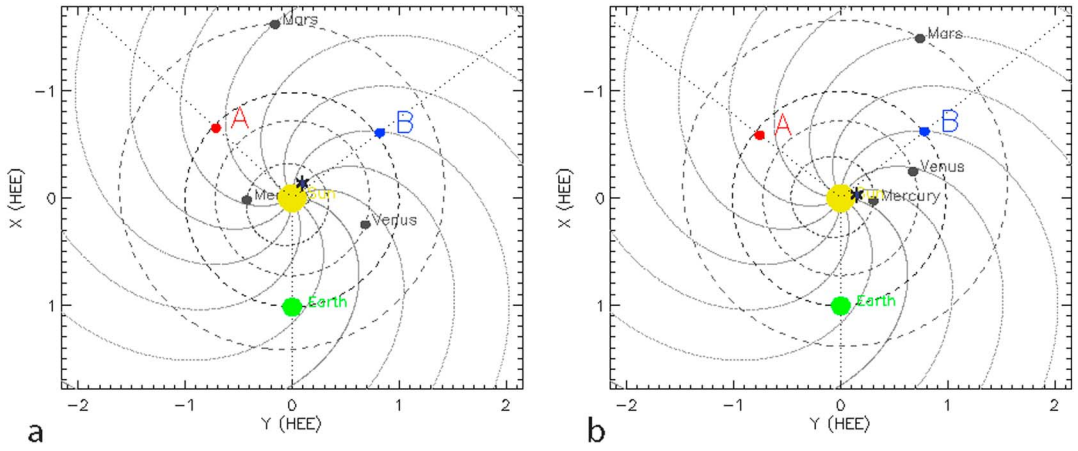

Figure 1. Inner solar system ecliptic plane settings of the planets and STEREO from the Stereo Science Center Orbit Tool (https://stereo-ssc.nascom.nasa.gov/where.shtml) for the July 2017 (a) and September 2017 (b) periods under study here. The asterisks mark the approximate centroids of the observed major eruptive activity in the corona.

models to interpret heliospheric events with the assumption that an observer's magnetic connection to an interplanetary shock is required for detection of the SEPs it generates. From the viewpoint of this approach, the time profile of the detected SEP fluxes reflect the time history of the observer's shock connections, together with the evolving strength of the connected shock source as it travels outward through the heliosphere. The modeled fluxes are also affected by the number of contributing shocks along the observer's field line if more than one SEP-producing shock is present in the ENLIL simulation, by observer-connected field line geometries that include magnetic mirrors and by the proximity of the magnetic field connection to the observer—which can bring with it an energetic storm particle (ESP) enhancement.

After assessing the coronal origins of the probable drivers of the SEP shock sources in late July 2017 and early September 2017, we discuss the WSA-ENLIL-cone model results and compare the associated SEPMOD SEP fluxes time series with observations. The results suggest that the eruptive activity from the same region of the corona in both July and September produced sequences of SEP-producing shocks with similar heliospheric patterns and thus similar patterns of SEP activity at Earth, STEREO-A, and Mars. This similarity is attributable to the occurrence of the multiple eruptions in roughly the same western heliolongitude quadrant, in the context of a coronal configuration that remained much the same throughout midlate 2017. Overall, these analyses with WSA-ENLIL-cone and SEPMOD provide an example of how postevent diagnostics can be carried out with these models, together with a view of the late cycle 24 activity illustrating how even near-minimum conditions sometimes produce significant space weather effects. Moreover, the attribution of the late cycle 23 (December 2006) activity to a similar cause (e.g., Kataoka et al., 2009) suggests that pseudostreamers may be a common host of late cycle activity in weak cycles such as 23 and 24.

2. Relevant Solar Events for July and September 2017

The WSA-ENLIL-cone heliospheric simulation (e.g., Odstrcil, 2003; Odstrcil et al., 2005; Mays et al., 2015) relies on the description(s) of CME activity seen in coronagraph and extreme ultraviolet images for inputs. These images are used to specify the parameters of an injected spherical volume of high pressure solar wind that represents the material ejected from the corona during the CME(s). In addition to the time of the ejection, critical parameters include the location of the eruption both on the Sun and at its passage through the 21.5 Rs (Rs = solar radius) inner boundary of ENLIL, the width of the ejected material as fit by the cone model (e.g., Zhao et al., 2002), and the inferred speed and direction of that material—taking into account the coronagraph's perspective. Having multiple perspectives from the combination of Earth and STEREO has been valuable for the purposes of determining these parameters, especially in cases such as those under study here where eruptions of interest occur on the farside as seen from Earth. Extreme Ultraviolet Imager recorded the on-disk eruption signatures including the related flares and coronal dimmings (see other papers in this special issue). Both Solar and Heliospheric Observatory Large Angle and Spectrometric Coronagraph

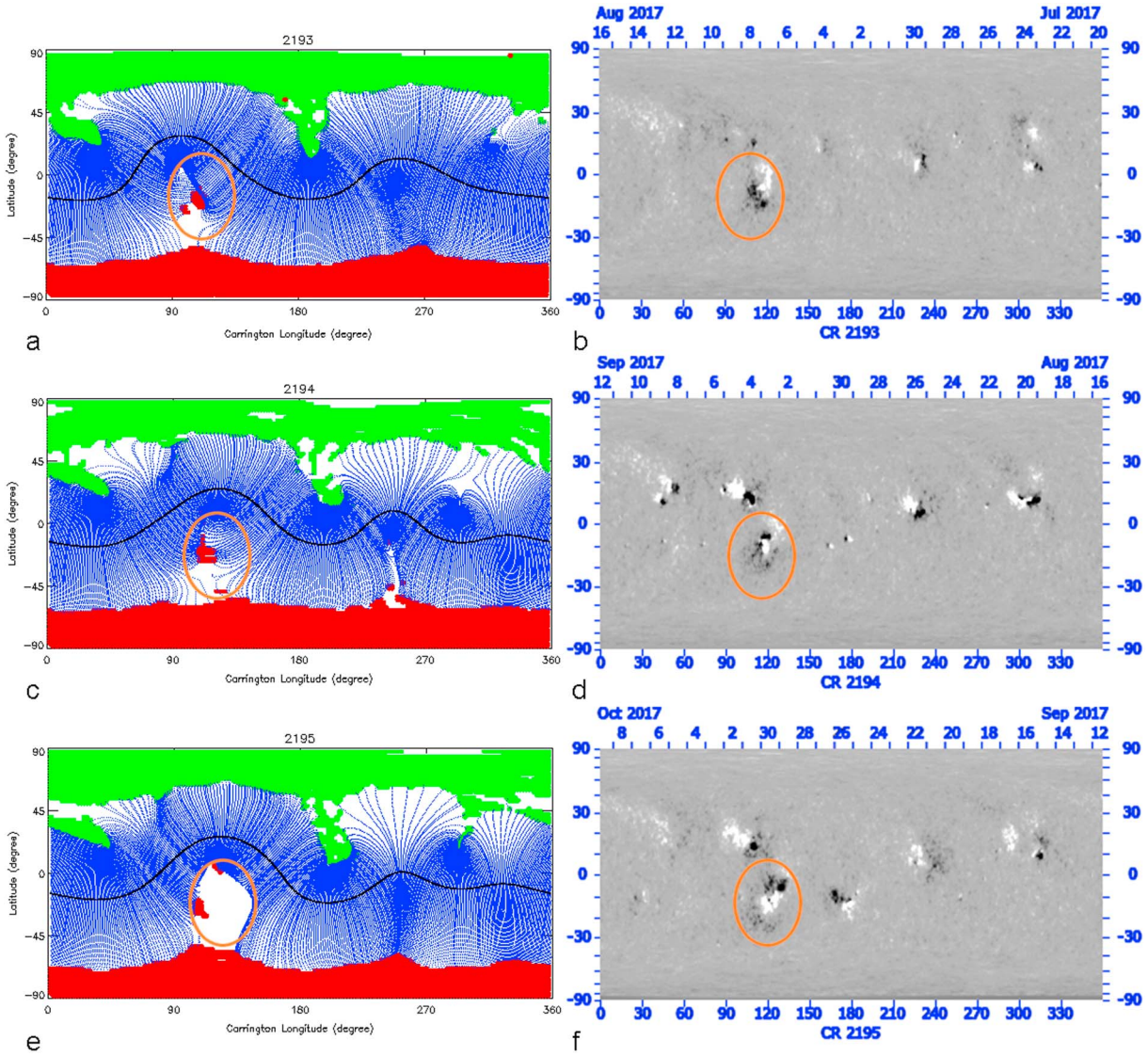

Figure 2. Panels (a, c, e): PFSS coronal magnetic field topologies based on the GONG synoptic maps in panels (b, d, f) for Carrington Rotations (CRs) 2193–2195. The green and red areas indicate the footprint of the open magnetic fields for the model, which has a source surface at 2.5 Rs. The blue lines are the closed field lines of the helmet streamer belt, with the source surface neutral line (black) along its crest. White areas in the PFSS maps are the footpoints of coronal pseudostreamers—self-contained, minaret-like closed field structures that stand outside the main helmet streamer arcade, often where the main streamer becomes "warped." The regions that gave rise to the coronal eruptions of July and September 2017 (circled) evolve to produce a pseudostreamer whose early stage is seen in panel (e). PFSS = Potential Field Source Surface.

(SOHO LASCO) and STEREO-A SECCHI COR1 coronagraphs captured the ejecta geometries and projected speeds from both perspectives. The coronal context of the events is suggested by the GONG Potential Field Source Surface (PFSS) model synoptic plots reproduced in Figures 2a and 2c. In this case the Carrington Rotation versions are shown to highlight the similar coronal helmet streamer and coronal hole structure occurring during both months. The area where the major eruptions originated is indicated, while the underlying GONG magnetic field maps showing the involved active region(s) are reproduced in Figures 2b and 2d. It is notable that the erupting region is located near the edge of the PFSS model closed field arcade (blue), in a warp in the main streamer belt. Following the eruptive activity, this area evolves into an initially small pseudostreamer (Figures 2e and 2f show the subsequent Carrington Rotation PFSS model and GONG map) whose footprint grows over subsequent months as the active region decays and spreads in area.

Table 1
*(a) Cone Model Parameters** for July 2017 Case. (b) Cone Model Parameters** for September 2017 Case*

	CME start time (UT)	Radial speed (km/s)	HEEQ longitude (°)	HEEQ latitude (°)	Half-width (°)
1	2017-07-12 14:00	430	27	8	37
2	2017-07-14 01:36	1,300	38	-8	54
3	2017-07-23 01:36	1,080	149	15	36
4	2017-07-23 04:39	1,900	−165	−12	58
5	2017-07-28 05:36	880	−131	5	41
	CME start time (UT)	Radial speed (km/s)	HEEQ longitude (°)	HEEQ latitude (°)	Half-width (°)
1	2017-09-04 20:36	1,325	4	−8	52
2	2017-09-04 19:39	830	23	−8	28
3	2017-09-06 12:24	1,850	24	−15	50
4	2017-09-06 13:09	1,180	99	−4	30
5	2017-09-09 16:48	480	100	−10	33
6	2017-09-09 23:12	700	105	5	41
7	2017-09-10 16:09	2,500	108	−9	90[a]
8	2017-09-17 12:09	1,600	−155	−5	54

Note. CME = coronal mass ejection; HEEQ = Heliocentric Earth Equatorial.
[a]The 2017-09-10 16:09 CME half-width was measured to be around 58°; however, we used the full-shock half width of 90° in the simulation, with a decreased overall CME density to approximate the CME shock. [b]These parameters refer to the projected location, speed, and size of the cone model CME at the 21.5 Rs position of the ENLIL simulation inner boundary rather than the low coronal characteristics.

The main eruptions for the July and September event periods were multiple in both cases, with at least two fast (>1,000 km/s) and wide (>90°) ejections following one another by roughly a week in each case—with the CME ejecta headed first to the west of Earth and then later in the general direction of Mars. These and several other moderate eruptions occurring within a ~20-day time period were modeled to obtain cone model parameter fits and then included in WSA-ENLIL-cone simulation runs for July and September 2017 as summarized in Tables 1a and 1b.

3. ENLIL With SEPMOD Approach

The ENLIL (WSA-ENLIL-cone) MHD simulation (Odstrcil, 2003; Odstrcil et al., 2005) is widely known and used in space weather applications (e.g., Mays et al., 2015)—with the result that the literature includes many descriptions of its design and attributes, and examples of its application. The particular ENLIL runs used here are based on GONG synoptic magnetic field maps that are updated every ~2 hr by the introduction of new disk images. The main additional development of ENLIL related to the SEP event modeling described here consisted of the ability to identify and characterize (in terms of MHD variables) the shocks generated by the cone-model CME disturbances (e.g., see Bain et al., 2016). As a result, the available outputs of ENLIL at the CCMC in selected "SEPMOD" runs include files that contain time sequences of observer heliospheric field lines saved at a ~5-min cadence, together with files describing any shocks on those field lines (one file for each observer for each CME included in the ENLIL run). Another modification for the SEPMOD-related ENLIL runs is the extension of the typical run periods to cover several weeks and out to heliocentric distances of ~5 AU. One caveat is that the 21.5 Rs inner boundary of ENLIL currently limits the ability to include the coronal portions of the fields and shocks and must be kept in mind when evaluating these simulations.

The details of how the SEPMOD SEP event model uses these ENLIL results have been discussed in several earlier papers (Luhmann et al., 2007, 2010, 2017) where the latter demonstrated applications to a number of multipoint SEP events obtained through the STEREO era. Briefly, the SEPMOD approach involves the time integration of a series of SEP injections from shocks on the sequential observer-connected interplanetary field lines. SEPMOD uses a test particle, guiding center approximation to follow protons, isotropically injected along each ENLIL field line at the shock position, for a specified number of time steps. This treatment naturally includes magnetic focusing and mirroring along the field lines (e.g., see Odstrcil & Pizzo, 1999 for a discussion of CME effects on ENLIL field lines). SEPMOD's procedure is applied to the 1- to 100-MeV proton energy range for evaluation purposes, although the assumptions are expected to be most appropriate for >10-MeV

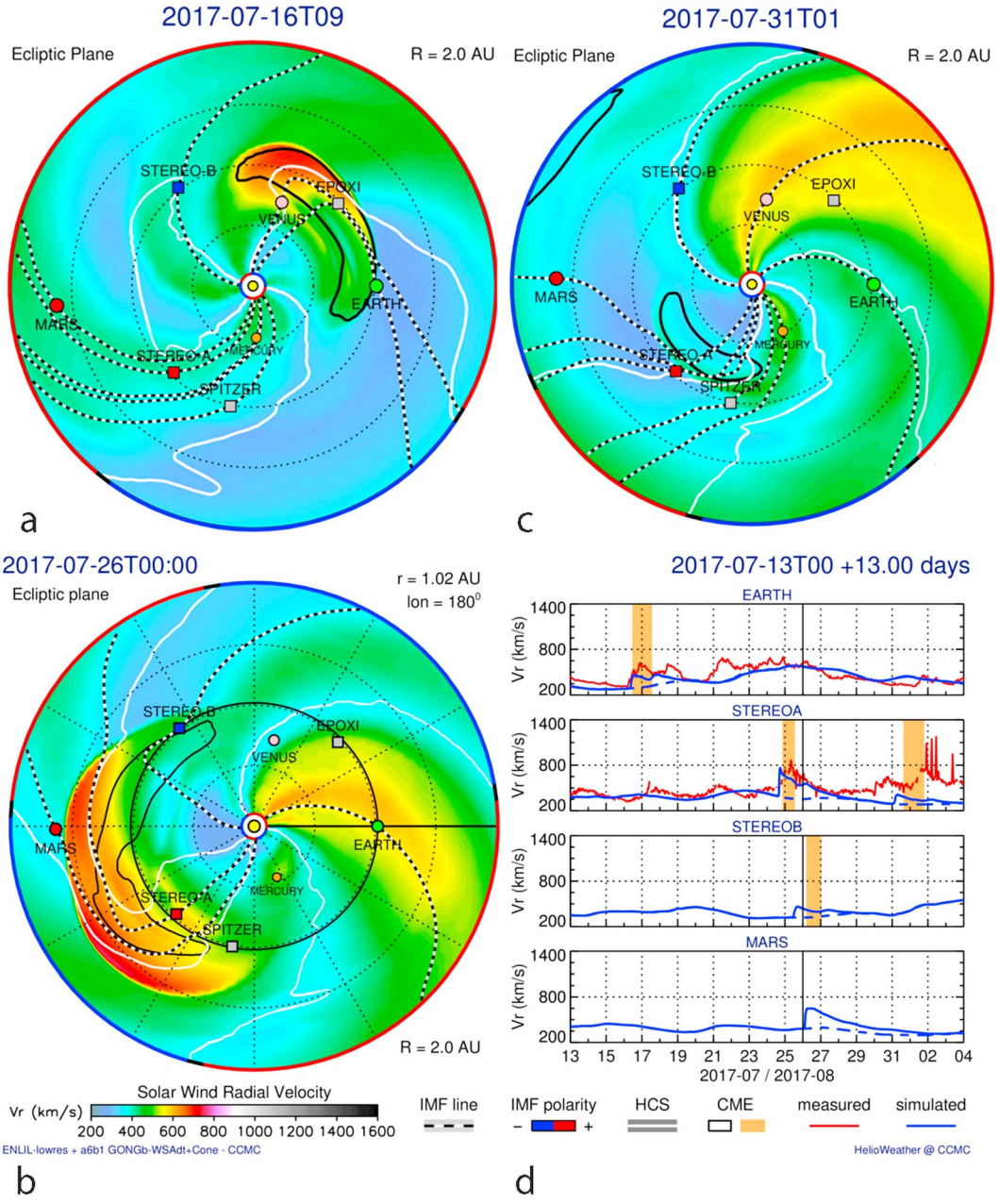

Figure 3. WSA-ENLIL-cone model results for the July 2017 event period, showing three snapshots (a–c) of the ecliptic solar wind radial velocity contours during the eruptions on the top and lower left, and in the lower right (d) the simulated time series (blue) of the radial velocities at observer sites including earth, STEREO-A and B, and Mars. The contour plots include the observer field lines (dashed) and the outline of cone model CME evolved "ejecta" (solid line). The time of the snapshot in panel (b) is indicated on the right in (d) by a vertical black line. Gold-shaded areas on the time series plot mark the passage of the cone model injected CME high pressure plasma. Red points show the corresponding velocity observations for those observer sites where solar wind plasma data are available. CME = coronal mass ejection; HCS = heliospheric current sheet; IMF = interplanetary magnetic field.

particles. The injected proton energy spectrum is a power law $KE^{-\gamma}$. Here E is the particle energy, and the power law index γ is given by $\gamma = 0.5(d + 2)/(d - 1)$ with d equal to the ENLIL-derived shock compression ratio at the observer field line connection. This spectral dependence arises from the theoretical analysis of the process of diffusive shock acceleration (e.g., see Jones & Ellison, 1991). The particle injection flux factor K is set by a scaling relation empirically determined by Lario et al. (1997, 1998), in which the log of the flux

varies in proportion to the shock velocity jump. An additional $1/r^2$ factor is added to incorporate the spherical expansion of the expanding volume represented by the ENLIL field line. If the observer connection is within a few tenths of an AU of a shock moving at over 300 km/s, a softer spectrum, observationally inspired ESP flux enhancement is added to the source strength description in SEPMOD that increases to a maximum at the shock location. All particle scattering of importance is presumed to occur at the shock source in the current SEPMOD scheme and is not otherwise included in the guiding center motion calculations. The end result is an observer's SEP time profile that is a reflection of the combination of their evolving field line connections to the shock and the strength of the shock (both the ENLIL plasma density compression ratio and velocity jump) at those connections. Note that because SEPMOD results are so highly dependent on the heliospheric description used, the importance of the WSA-ENLIL-cone CME model accuracy cannot be overstated.

4. Results

4.1. Event Period ENLIL Results

Figures 3 and 4 show snapshots from the ENLIL runs made for the July and September 2017 study periods in the form of ecliptic plane color contour plots of the plasma velocity at a selected time in the simulations (top and lower left panels) and modeled time series of the radial velocity at several observer locations (lower right). The relative positions of the three observers considered here (also shown in Figures 1a and 1b) at Earth, STEREO-A, and Mars, are superposed on the velocity contour plots together with the magnetic field lines that thread through them at the time of the snapshots. The modeled time series on the right show the arrival times of the simulated ICMEs at the observers (including the currently not operational STEREO-B) as jumps in speed that are followed by gold shaded intervals indicating the times and durations of the passage of the cone model CME high pressure plasma. These represent the periods where the CME ejecta structures such as flux ropes—not in the ENLIL simulations used here—would be observed. Available observations of the solar wind velocities from ACE (McComas et al., 1998) and STEREO-A (Galvin et al., 2008) are also superposed for comparison.

Due to the similar relative observer positions for Earth, STEREO-A, and Mars during the summer/fall of 2017, it is useful to think of them as stationery heliospheric beacons while the active region is emitting CMEs as it rotates in a right-handed direction with the ~27-day period of the Sun. The July 2017 case (Figure 3) includes 22 days during which a moderately strong first shock and its CME driver from a western disk CME impacted Earth on 16 July, followed by a stronger, faster encounter with a subsequent, larger ejection at STEREO-A on 24 July. Roughly a day later the same disturbance passed both STEREO-B and Mars—although the broad nature of this ejection and its interaction with the ambient solar wind stream structure made the simulated passage of the driver by Mars somewhat ambiguous. At this time the active region that had produced the Earth event, was located roughly ~120° over the west limb, in-line with STEREO-A and Mars. Late in the simulated interval another weaker, slower shock and its driver went past STEREO-A. All of these ejections appear to have come from the vicinity of the same active region mentioned earlier, and so the related cone CMEs were sequentially launched from its increasingly westward site as the Sun rotated and as inferred from the coronagraph images. The simulated velocities and shock arrivals appear to capture the basic features of what is observed, providing a measure of the inner heliosphere-wide accuracy of this ENLIL run.

The analogous period in September 2017 (Figure 4), almost exactly two solar rotations later, similarly starts with an early event detection at Earth in 7 and 8 September—actually a close sequence of a weak event followed by a stronger one—including the passage of two shocks and their drivers. The subsequent event about 5 days later this time impacts STEREO-B and Mars because the active region was not as far around the limb. Also, a last, weaker ejection again is directed toward STEREO-A. Note that although the temporal and spatial sequences are somewhat shifted with respect to one another, both the July and September 2017 cases have in common the coronal setting of the CME-producing active region (Figures 2a, 2c, and 2e), together with the onset of a ~20-day period of activity starting with a significant Earth-impacting event, followed within days by a sequence of further eruptions that impact the observers in the western and then farside heliosphere as the Sun rotates. In both cases the later activity includes a wide, fast Mars-directed event. As such, it hints at a possibly homologous behavior involving the same coronal region and heliolongitude sector. Whether the initial eruptions toward Earth destabilized the remaining nearby structure or ongoing evolution of the active region and surrounding coronal structure resulted in

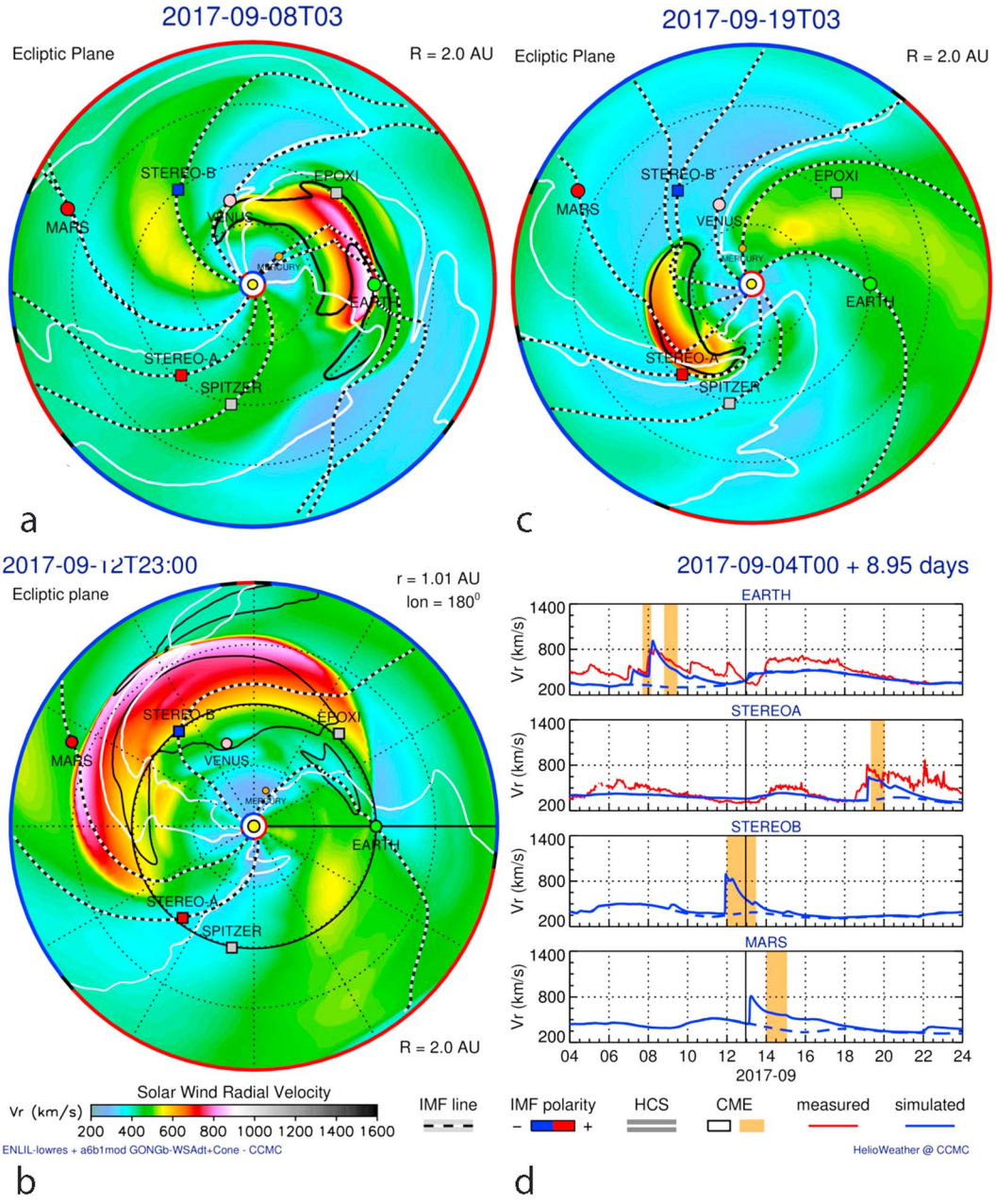

Figure 4. Same as Figure 3 but for 4–24 September 2017. CME = coronal mass ejection; HCS = heliospheric current sheet; IMF = interplanetary magnetic field.

explosive adjustments is not clear. However, since the STEREO mission was launched in 2006, it has observed a number of several week-long periods of multiple CMEs, with ICMEs that overlap in time and space—sometimes from the same major active region as in this case and sometimes over several solar rotations (e.g., examples in Luhmann et al., 2017). The "active longitude sector" nomenclature is probably appropriate in some of these cases as well. Why in this case the activity seems to have skipped the August rotation is likely worth closer examination.

4.2. Observed and Modeled SEP Time Profiles

In considering the results in Figures 3 and 4, note that the SEPs at an observer's location may come from remote connections to CME-driven shocks that are not detected in situ. Thus, SEP time series behavior

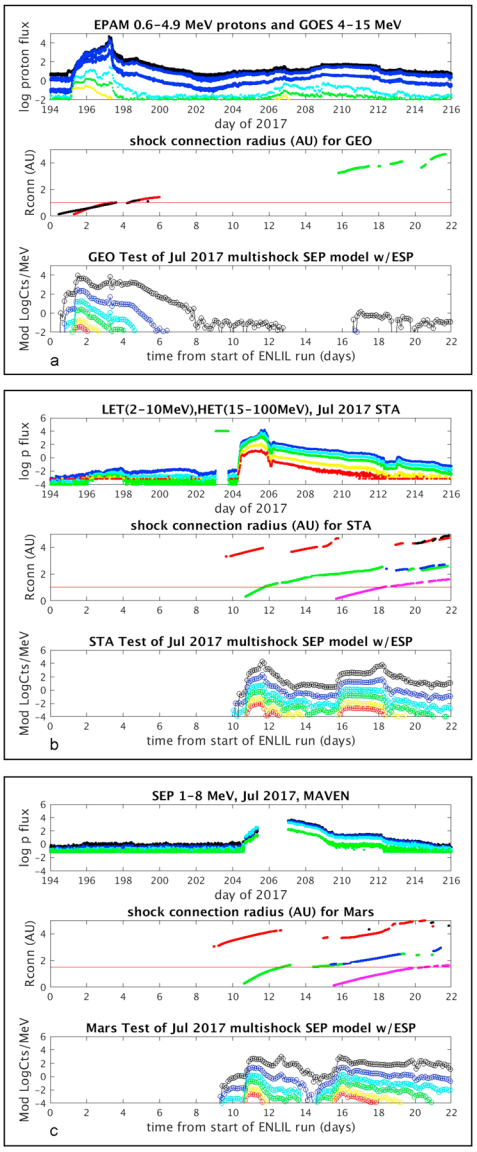

Figure 5. (a; top panel) Time series of the SEP activity observed in July 2017 as seen in ACE and GOES 1- to 100-MeV energetic protons (top panel, fluxes in units of protons/[cm^2·s·sr·MeV]); (middle panel) ENLIL results for the simulated interplanetary coronal mass ejection shocks during this period, showing the heliocentric radius of the (Earth-GEO) observer (red line) and the radius Rconn of the field line connection to each shock (distinguished by color; middle panel); and (lower panel) the results of the SEPMOD calculations for a proton energy range similar to the data and on the same (log) differential flux scale, based on the ENLIL results. Note the timescale for the data in the top panel is in day of year, while the timescale for the two model panels below is the time from the start of the ENLIL run. In both the data and model time series, black represents the lowest energies ~1 MeV and red the highest energies. The model time series are for the SEPMOD default energy "channels" at 1.2, 2.6, 5.1, 8.6, 17, and 26 MeV. (b, c) Same as (a) but for STEREO-A (STA) and MAVEN (Mars) whose locations relative to earth at this time can be seen in Figures 1a and 3. EPAM = Electron Proton Alpha Monitor; ESP = energetic storm particle; GOES = Geostationary Operational Environmental Satellite Program; HET = High-Energy Telescope; LET = Low-Energy Telescope; MAVEN = Mars Atmosphere and Volatile EvolutioN; SEP = solar energetic particle; STEREO = Solar TErrestrial RElations Observatory.

may not necessarily be inferred from the in situ plasma and field behavior alone. Observer field lines can also intersect more than one ICME at a particular time, leading to multiple source contributions and possible magnetic mirroring effects in the SEPMOD results. An important consideration here is that it is difficult to evaluate the ENLIL results solely from their behavior at an observer's location. In contrast, SEP time profiles present a kind of long-baseline, remote probe of the heliosphere—albeit over a limited spatial volume.

Figures 5 and 6 show SEPMOD results for the selected event periods (bottom panels), together with 5-min-resolution SEP proton observations from STEREO-A (abbreviated in the plots by STA) Low- and High-Energy Telescopes (Mewaldt et al., 2008; von Rosenvinge et al., 2009), Electron Proton Alpha Monitor (EPAM) on ACE (Gold et al., 1998), and GOES EPS fluxes (1-hr resolution) from the OMNI database (https://omniweb.gsfc.nasa.gov; top panels), and MAVEN's SEP detector (Larson et al., 2015). The time spans covered by the ENLIL runs for these cases are ~20 days. Separate plots represent the three observer locations. The observed SEP time series are plotted for different ranges of proton energies from ~1 to ~100 MeV, while the corresponding SEPMOD plots in the bottom panels show calculated counterparts on the same flux scale as the observations. However, for the display of the model results we use a fixed, uniform sampling in proton energy over the range that covers the observations shown, with similar colors used for similar energies.

The middle panels are useful for interpreting the SEP time series in terms of the heliocentric radius (Rconn) of the observer magnetic connections to the shock from each ENLIL CME (distinguished by color). These also indicate the relative timings of the shock connections, which may not coincide with the time(s) of the CME(s) and/or ICME(s)—see Table 1 and Figures 3 and 4. The horizontal red lines mark the nominal observer heliocentric distance. Shock connections located below this observer line occur between the ENLIL inner boundary at 21.5 Rs and the observer location, while connections above it occur outside the observer location up to the ENLIL outer boundary. Notice that the time spent connected to shocks beyond the observer may exceed the time spent connected inside. Traces that cross the red line (as seen in the Rconn panels in Figures 5 and 6), indicate that the in situ observer should experience the shock passage and the related ESP enhancement in the observer's SEP time profiles. In both the July and September cases the Earth shock connections start near the inner ENLIL boundary (near Rconn = 0 on this plot). In contrast, the later events at STEREO-A and Mars include one or more long-lived connections to distant shocks. However, the contributions of these outside shock connections are considerably diminished compared to the overlapping inner connections, including some near-Sun connections. In general, ICME shocks weaken with heliocentric distance beyond a few 10s of solar radii, leading to domination of such combined events by the innermost heliospheric shocks.

5. Discussions

As can be seen from Figures 1a and 3, STEREO-A and Mars were especially well aligned along the same nominal Parker Spiral field line for the July 2017 event period. This explains the very similar observer

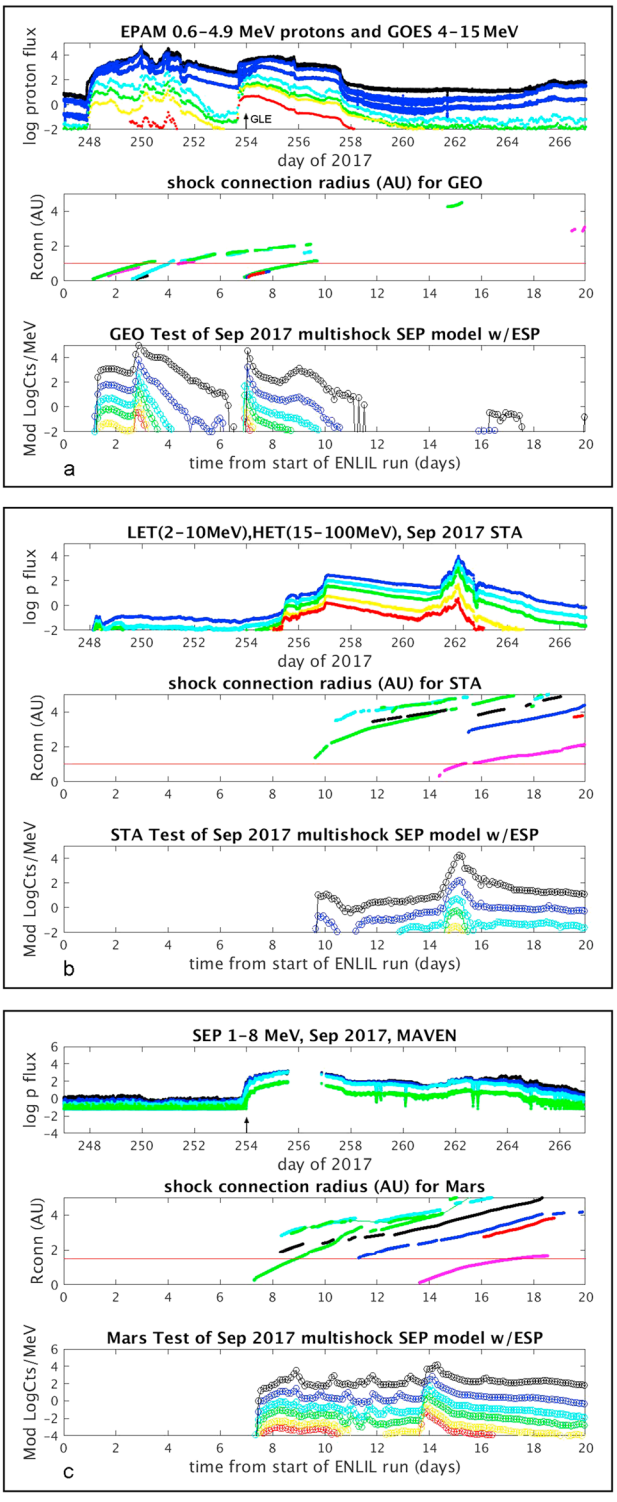

Figure 6. Same as Figure 5 but for the September 2017 event period. The locations of the three observing points at this time for (a) Earth (GEO), (b) STEREO-A (STA), and (c) Mars (MAVEN) can be seen in Figures 1b and 4. EPAM = Electron Proton Alpha Monitor; ESP = energetic storm particle; GOES = Geostationary Operational Environmental Satellite Program; HET = High-Energy Telescope; LET = Low-Energy Telescope; MAVEN = Mars Atmosphere and Volatile EvolutioN; SEP = solar energetic particle; STEREO = Solar TErrestrial RElations Observatory.

shock connection radius histories and calculated event time profiles at these two sites in Figures 5b and 5c (middle and bottom panels). The comparison of the calculated SEP events in the bottom panels with the observed SEP events in the top panels seems to be in better agreement for STEREO-A although the MAVEN SEP data at Mars cover a smaller energy range and have a data gap near the peak flux. MAVEN has been in orbit around Mars since late 2014 (Jakosky et al., 2015) with a payload that includes a plasma and field detectors in addition to the SEP instrument which detects SEP ions (~20 to ~6 MeV) and electrons (~20 to ~200 keV; see Larson et al., 2015). Several challenges with the use of these data from a Mars orbiter include a restricted field of view that is regularly reoriented to accommodate other Mars observations as well as perturbations to the local interplanetary environment by Mars itself, which absorbs SEPs (e.g., Lillis et al., 2016). Nevertheless the regular availability of these data at the Mars location enables studies of the radial evolution of SEP events including the ability to infer Mars event characteristics from the more common 1-AU observations.

The September 2017 event(s) produced one of the strongest space environment storms observed on MAVEN since 6 March 2015, with the most intense SEP fluxes yet detected (e.g., see Lee et al., 2017; upcoming special issue of Geophysical Research Letters). This case also included one of the relatively rare observations by the MSL RAD detector of a surface SEP event (for discussion of these phenomena at Mars see Hassler et al., 2014). At about the same time, Earth observations on 10 September 2017 showed a ground level event (GLE) that is often associated with a western disk, near-Sun shock connection (timing indicated by the arrow in the top panel of Figure 6a). The same coronal region apparently produced broad and/or sequential coronal shocks that made particularly energetic (>100 MeV at Earth) contributions to the event(s) seen at both Earth and Mars. Their mutual magnetic connection to the same near-Sun shock in the ENLIL simulation is suggested here by the green shock connection radial distance traces in Figures 6a and 6c on day 254 (11 September). Considering the timing of these events near the end of the declining phase of the current solar cycle, this is worth noting for future space environment planning for human exploration.

In both of these modeled cases (Figures 5 and 6), the similarity of the modeled time series of SEP fluxes to the observations supports the basic assumption in SEPMOD that an observer's magnetic field connection to the CME-driven shock is a key factor in the occurrence (or not) of a local SEP event. While the importance of cross-field (perpendicular) diffusion during SEP transport remains a subject of research (e.g., Zhang et al., 2003), these results lend further weight to the argument that the role of diffusive motion in SEP event longitudinal spread should be evaluated only after the observers' shock magnetic connection history is understood. In addition, the apparently frequent occurrence of an observer's magnetic connections to multiple shocks at the same time (see middle panels in Figures 5 and 6) is important in considering flux contributions from earlier events (sometimes referred to as seed particles), as well as sorting out potential confusion in interpreting SEP events produced when overlapping CME-driven shocks are present. This implies that SEP modeling of real events without a corresponding realistic heliospheric model is unlikely to yield desired insights.

Another aspect of these events worth considering is their occurrence following a relatively weak active phase and their apparent coronal pseudostreamer association. The situation at the end of solar cycle 24 is similar to that at the end of cycle 23, where large and persistent pseudo-streamers seem to be occurring related to the weak polar fields (e.g., see Petrie, 2012). It is generally the case during the descending phases of cycles that the trailing polarities of late-appearing active regions' effective magnetic "bipoles" match the polar field's polarity in each hemisphere, with the trailing polarity systematically closer to the pole than the leading polarity (Joy's law). This leads to and reinforces the polar field reversals as the active regions decay and their flux is transported by poleward flows. However, active region bipole tilts of anomalous sign or minimal tilts would weaken a newly reversing polar field, setting up the conditions for warping of the main streamer belt and formation of pseudostreamers. The weakness of the cycle 23 polar fields was due to the active regions producing a mixture of like- and opposite-polarity surges arriving at the poles during this time, inhibiting the development of stronger polar fields. It is likely that the weakening of the polar fields in the latest cycle, together with the appearance of large pseudostreamers in the declining phase, are the consequences of its similar surface flux development patterns.

CMEs arising from pseudostreamers are sometimes considered to have only weak-to-moderate ejection characteristics including speed and generally narrower widths (e.g., Wang, 2015). However, the major CMEs in this case were quite wide and fast (see Table 1). While the event-related pseudostreamer in the PFSS models for this study period became noticeable mainly after the major eruptions (see its white "footprint" in Figure 2e), the field geometry is likely to have been already present at the site in nonpotential form. Considering that overlying coronal field arcades are thought to represent a barrier to underlying active region eruptions (e.g., Torok & Kliem, 2007), the cusp-like field structures of pseudostreamers topped by magnetic nulls are possibly less constraining than the main streamer belt. The matter of pseudostreamer eruptivity is one area in the investigations into CME initiation processes (e.g., Lynch & Edmondson, 2013) that may be especially timely in the present cycle—and also impacts the assessments of prospective SEP sources.

Li et al. (2012) have argued that pseudostreamers can be particularly auspicious settings for the generation of GLEs, the most energetic SEP events in terms of the hardness of their energy spectra (e.g., see Cohen et al., 2017). Their reasoning involves the likelihood of sympathetic eruptions of adjacent portions of the streamers' interior arcades, thus enabling SEP interactions with multiple shocks in these settings. On the other hand, Kahler and Vourlidas (2014) examined their own set of such events and suggest that simply the presence of multiple shocks and the SEPs they produce in the same neighborhood could be responsible for the associated high intensities. The examples shown here appear consistent with this second interpretation, where overlapping events combined with mirroring/trapping in the generally disturbed heliospheric fields produce apparently strong and long-lived events.

6. Concluding Remarks

The solar activity outbursts in July and September 2017, near the end of the present cycle 24 declining phase, sparked interest due to their apparently energetic nature near the end of a relatively weak solar active phase. These events also highlight the potential for coronal pseudostreamers sites associated with active regions to spawn substantial eruptions giving rise to large, widespread SEP fluxes and even GLEs. Weak activity cycles appear to encourage the formation of pseudostreamers because the higher-order harmonics of the coronal magnetic field become more important relative to the low-order harmonics usually related to the solar polar fields (e.g., Petrie, 2012). Further episodes of similar nature before the end of cycle 24, and even into the solar minimum, cannot be ruled out.

The above examples also once again raise the issue of SEP event forecasting and whether it is presently achievable with tools such as the combination of ENLIL and SEPMOD used here. While SEPMOD can in principle be run in a few minutes on "real-time" ENLIL results produced at the Goddard Space Flight Center Space Research Center (jttps://ccmc.gsfc.nasa.gov/iswa/), the accuracy of those real-time ENLIL runs has yet to be fully evaluated. The retrospective adjustments made to the ENLIL (and thus related SEPMOD) runs used here benefited from reassessments of the cone model CME parameters based on both ENLIL-simulated time series comparisons to solar wind observations and shock arrival times, and the SEP observations. In particular, reliance on automated methods for deducing cone model CME parameters from real-time coronagraph images without human intervention provides a challenge. Nevertheless, ensemble approaches (e.g., Lee et al., 2013;

Mays et al., 2015) in which a number of ENLIL runs are generated and used with SEPMOD for the period of interest may at least bracket the range of possible outcomes.

Acknowledgments
The authors are grateful to the staff of the CCMC for their contributions to deriving the ENLIL cone model parameters, to the SOHO LASCO and STEREO SECCHI investigators for the coronagraph images used, to the GONG Observatory for providing the magnetic synoptic maps used for the ambient solar wind description, to the ACE and STEREO plasma investigation teams for providing 1-AU solar wind data shown here, to the ACE EPAM and GOES EPS Instrument and data providers, and to the MAVEN and Venus Express projects for providing data for the planetary site SEP event-model comparisons. This work was supported in part by NASA grant NNX15AG09G to the University of California, Berkeley for the STEREO-IMPACT investigation and by NASA grant NNX15AUo1G to the University of New Hampshire for the STEREO PLASTIC investigation. Additional support for the Caltech contributions is from NSF grant 1156004. The model development at UC Berkeley is sponsored by the NSF Award 1322826 through the Living With a Star Program in cooperation with NASA. M. L. M., H. B., and Y. L. acknowledge the support of NASA LWS grant NNX15AB80G. WSA-ENLIL+Cone simulation results have been provided by the Community Coordinated Modeling Center at the Goddard Space Flight Center through their public Runs on Request system (http://ccmc.gsfc.nasa.gov; run numbers Leila_Mays_080917_SH_1, Leila_Mays_120817_SH_9). The WSA model was developed by N. Arge at AFRL, and the ENLIL Model was developed by D. Odstrcil at GMU.

References

Bain, H. M., Mays, M. L., Luhmann, J. G., Li, Y., Jian, L. K., & Odstrcil, D. (2016). Shock connectivity in the August 2010 and July 2012 solar energetic particle events inferred from observations and ENLIL modeling. *The Astrophysical Journal*, *825*(1), 22. https://doi.org/10.3847/0004-637X/825/1/1

Cohen, C. M. S., Luhmann, J. G., Mewaldt, R. A., Mays, M. L., Bain, H. M., Li, Y., & Lee, C. O. (2017). Searching for extreme SEP events with STEREO, Proceedings 35th International Cosmic Ray Conference -ICRC2017, Busan, Korea, July 2017.

Galvin, A. B., Kistler, L. M., Popecki, M. A., Farrugia, C. J., Simunac, K. D. C., Ellis, L., et al. (2008). The Olasma and suprathermal ion composition (PLASTIC) investigation on the STEREO observatories. *Space Science Reviews*, *136*(1-4), 437–486.

Gold, R. E., Krimigis, S. M., Hawkins, S. E., Haggerty, D. K., Lohr, D. A., Fiore, E., et al. (1998). Electron, proton, and alpha monitor on the Advanced Composition Explorer spacecraft. *Space Science Reviews*, *86*, 541–562.

Hassler, D. M., Zeitlin, C., Wimmer-Schweingruber, R. F., Ehresmann, B., Rafkin, S., Eigenbrode, J. L., et al. (2014). Mars surface radiation environment measured with the Mars Science Laboratory's Curiosity rover. *Science*, *343*(6169), 1244797. https://doi.org/10.1126/science.1244797

Jakosky, B. M., Grebowsky, J. M., Luhmann, J. G., Connerney, J., Eparvier, F., Ergun, R., et al. (2015). MAVEN observations of the response of Mars to an interplanetary coronal mass ejection from the sun. *Science*, *350*(6261), aad0210. https://doi.org/10.1126/science.aad0210

Jones, F. C., & Ellison, D. C. (1991). The plasma physics of shock acceleration. *Space Science Reviews*, *58*, 259–346.

Kahler, S. W., & Vourlidas, A. (2014). Do interacting coronal mass ejections play a role in solar energetic particle events? *The Astrophysical Journal*, *784*(1), 47. https://doi.org/10.1088/0004-637X/784/1/47

Kaiser, M. L., Kucera, T. A., Davila, J. M., St. Cyr, O. C., Guhathakurta, M., & Christian, E. (2008). The STEREO mission: An introduction. *Space Science Reviews*, *136*, 5–16.

Kataoka, R., Ebisuzaki, T., Kusano, K., Shiota, D., Inoue, S., & Yamamoto, T. T. (2009). Three dimensional MHD modeling of the solar wind structures associated with 13 December 2006 coronal mass ejection. *Journal of Geophysical Research*, *114*, A10102. https://doi.org/10.1029/2009JA014167

Lario, D., Sanahua, B., & Heras, A. M. (1997). Modeling the interplanetary propagation of 0.1-20 MeV shock accelerated protons II: Energy spectrum and evolution of the injection rate. *Advances in Space Research*, *20*(1), 121–126.

Lario, D., Sanahuja, B., & Heras, A. M. (1998). Energetic particle events: Efficiency of interplanetary shocks as 50 keV $<$ E $<$ 100 MeV proton accelerators. *The Astrophysical Journal*, *509*(1), 415–434.

Larson, D. E., Lillis, R. J., Lee, C. O., Dunn, P. A., Hatch, K., Robinson, M., et al. (2015). The MAVEN solar energetic particle investigation. *Space Science Reviews*, *195*(1-4), 153–172.

Lee, C. O., Arge, C. N., Odstrcil, D., Millward, G., Pizzo, V., Quinn, J. M., & Henney, C. J. (2013). Ensemble modeling of CME propagation. *Solar Physics*, *285*(1-2), 349–368.

Lee, C. O., Hara, T., Halekas, J. S., Thiemann, E., Chamberlin, P., Eparvier, F., et al. (2017). MAVEN observations of the solar cycle 24 space weather conditions at Mars. *Journal of Geophysical Research: Space Physics*, *122*, 2768–2794. https://doi.org/10.1002/2016JA023495

Li, G., Moore, R., Mewaldt, R. A., Zhao, L., & Labrador, A. W. (2012). A twin CME scenario for ground level enhancement events. *Space Science Reviews*, *171*, 141–160.

Lillis, R. J., Lee, C. O., Larson, D., Luhmann, J. G., Halekas, J. S., Connerney, J. E., & Jakosky, B. M. (2016). Shadowing and anisotropy of solar energetic ions at Mars measured by MAVEN during the March 2015 solar storm. *Journal of Geophysical Research: Space Physics*, *121*, 2818–2829. https://doi.org/10.1002/2015JA022327

Luhmann, J. G., Ledvina, S. A., Krauss-Varban, D., Odstrcil, D., & Riley, P. (2007). A heliospheric simulation-based approach to SEP source and transport modeling. *Advances in Space Research*, *40*(3), 295–303.

Luhmann, J. G., Ledvina, S. A., Odstrcil, D., Owens, M. J., Zhao, X.-P., Liu, Y., & Riley, P. (2010). Cone model-based SEP event calculations for applications to multipoint observations. *Advances in Space Research*, *46*(1), 1–21.

Luhmann, J. G., Mays, M. L., Odstrcil, D., Yan, L., Bain, H., Lee, C. O., et al. (2017). Modeling solar energetic particle events using ENLIL heliospheric simulations. *Space Weather*, *15*, 934–954. https://doi.org/10.1002/2017SW001617

Lynch, B. J., & Edmondson, J. K. (2013). Sympathetic magnetic breakout coronal mass ejections from pseudostreamers. *Astrophysical Journal*, *764*(1), 87. https://doi.org/10.1088/0004-637X/764/1/87

Mays, M. L., Taktakishvili, A., Pulkkinen, A., MacNeice, P. J., Rastätter, L., Odstrcil, D., et al. (2015). Ensemble modeling of CMEs using th WSA-ENLIL+Cone model. *Solar Physics*, *290*(6), 1775–1814.

McComas, D. J., Bame, S. J., Barker, P., Feldman, W. C., Phillips, J. L., Riley, P., & Griffee, J. W. (1998). Solar Wind Electron Proton Alpha Monitor (SWEPAM) for the Advanced Composition Explorer. *Space Science Reviews*, *86*(1/4), 563–612.

Mewaldt, R. A., Cohen, C. M. S., Cook, W. R., Cummings, A. C., Davis, A. J., Geier, S., et al. (2008). The Low-Energy Telescope (LET) and SEP central electronics for the STEREO mission. *Space Science Reviews*, *136*(1-4), 285–362.

Odstrcil, D. (2003). Modeling 3D solar wind structure. *Advances in Space Research*, *32*(4), 497–506. https://doi.org/10.1016/S0273-1177(03)00332-6

Odstrcil, D., & Pizzo, V. J. (1999). Distortion of the interplanetary magnetic field by three dimensional propagation of coronal mass ejections in a structures solar wind. *Journal of Geophysical Research*, *104*(A12), 28,225–28,239. https://doi.org/10.1029/1999JA900319

Odstrcil, D., Pizzo, V. J., & Arge, C. N. (2005). Propagation of the 12 May 1997 interplanetary coronal mass ejection in evolving solar wind structures. *Journal of Geophysical Research*, *110*, A02106. https://doi.org/10.1029/2004JA010745

Petrie, G. J. D. (2012). Evolution of active and polar photospheric magnetic fields during the rise of cycle 24 compared to previous cycles. *Solar Physics*, *281*(2), 577–598. https://doi.org/10.1007/s11207-012-0117-3

Richardson, I. G., von Rosenvinge, T. T., Cane, H. V., Christian, E. R., Cohen, C. M. S., Labrador, A. W., et al. (2014). $>$ 25 MeV proton events observed by the high energy telescopes on the STEREO A and B spacecraft and/or at the Earth during the first ~seven years of the STEREO mission. *Solar Physics*, *289*(8), 3059–3107. https://doi.org/10.1007/s11207-014-0524-8

Torok, T., & Kliem, B. (2007). Numerical simulations of fast and slow coronal mass ejections. *Astronomische Nachrichten*, *328*(8), 743–747. https://doi.org/10.1002/asna.200710795

von Rosenvinge, T. T., Richardson, I. G., Reames, D. V., Cohen, C. M. S., Cummings, A. C., Leske, R. A., et al. (2009). The solar energetic particle event of 14 December 2006. *Solar Physics*, *256*(1-2), 443–462. https://doi.org/10.1007/s11207-009-9353-6

Wang, Y.-M. (2015). Pseudostreamers as the source of a separate class of solar coronal mass ejections. *Astrophysical Journal Letters*, *803*(1), L12. https://doi.org/10.1088/2041-8205/803/1/L12

Zhang, M., Jokipii, J. R., & McKibben, R. B. (2003). Perpendicular transport of solar energetic particles in heliospheric magnetic fields. *The Astrophysical Journal*, *595*(1), 493–499.

Zhao, X. P., Plunkett, S. P., & Liu, W. (2002). Determination of geometric and kinematical properties of halo coronal mass ejections using the cone model. *Journal of Geophysical Research*, *107*(A8), 1223. https://doi.org/10.1029/2001JA009143